

## Original Article

# PET brain kinetics studies of $^{11}\text{C}$ -ITMM and $^{11}\text{C}$ -ITDM, radioprobes for metabotropic glutamate receptor type 1, in a nonhuman primate

Tomoteru Yamasaki<sup>1</sup>, Jun Maeda<sup>2</sup>, Masayuki Fujinaga<sup>1</sup>, Yuji Nagai<sup>2</sup>, Akiko Hatori<sup>1</sup>, Joji Yui<sup>1</sup>, Lin Xie<sup>1</sup>, Nobuki Nengaki<sup>3</sup>, Ming-Rong Zhang<sup>1</sup>

<sup>1</sup>Molecular Probe Program, Molecular Imaging Center, National Institute of Radiological Sciences, Inage-ku, Chiba, Japan; <sup>2</sup>Molecular Neuroimaging Program, Molecular Imaging Center, National Institute of Radiological Sciences, Inage-ku, Chiba, Japan; <sup>3</sup>Shi Accelerator Service Co. Ltd, Shinagawa-ku, Tokyo, Japan

Received February 24, 2014; Accepted March 13, 2014; Epub April 25, 2014; Published April 30, 2014

**Abstract:** The metabotropic glutamate receptor type 1 (mGluR1) is a novel target protein for the development of new drugs against central nervous system disorders. Recently, we have developed  $^{11}\text{C}$ -labeled PET probes  $^{11}\text{C}$ -ITMM and  $^{11}\text{C}$ -ITDM, which demonstrate similar profiles, for imaging of mGluR1. In the present study, we compared  $^{11}\text{C}$ -ITMM and  $^{11}\text{C}$ -ITDM PET imaging and quantitative analysis in the monkey brain. Respective PET images showed similar distribution of uptake in the cerebellum, thalamus, and cingulate cortex. Slightly higher uptake was detected with  $^{11}\text{C}$ -ITDM than with  $^{11}\text{C}$ -ITMM. For the kinetic analysis using the two-tissue compartment model (2-TCM), the distribution volume ( $V_t$ ) in the cerebellum, an mGluR1-rich region in the brain, was  $2.5 \text{ mL}\cdot\text{cm}^{-3}$  for  $^{11}\text{C}$ -ITMM and  $3.6 \text{ mL}\cdot\text{cm}^{-3}$  for  $^{11}\text{C}$ -ITDM. By contrast, the  $V_t$  in the pons, a region with negligible mGluR1 expression, was similarly low for both radiopharmaceuticals. Based on these results, we performed noninvasive PET quantitative analysis with general reference tissue models using the time-activity curve of the pons as a reference region. We confirmed the relationship and differences between the reference tissue models and 2-TCM using correlational scatter plots and Bland-Altman plots analyses. Although the scattergrams of both radiopharmaceuticals showed over- or underestimations of reference tissue model-based the binding potentials against 2-TCM, there were no significant differences between the two kinetic analysis models. In conclusion, we first demonstrated the potentials of  $^{11}\text{C}$ -ITMM and  $^{11}\text{C}$ -ITDM for noninvasive PET quantitative analysis using reference tissue models. In addition, our findings suggest that  $^{11}\text{C}$ -ITDM may be superior to  $^{11}\text{C}$ -ITMM as a PET probe for imaging of mGluR1, because regional  $V_t$  values in PET with  $^{11}\text{C}$ -ITDM were higher than those of  $^{11}\text{C}$ -ITMM. Clinical studies of  $^{11}\text{C}$ -ITDM in humans will be necessary in the future.

**Keywords:** Central nervous system (CNS), positron emission tomography (PET), metabotropic glutamate receptor type 1 (mGluR1)

## Introduction

Glutamate is the major excitatory neurotransmitter in the central nervous system (CNS), and exerts its actions on synaptic transmission by binding to the ionotropic and metabotropic glutamate receptor families. Metabotropic glutamate receptors (mGluRs) are G protein-coupled receptors [1], and include eight subtypes (mGluR1-8) divided into three groups based on sequence homology, intracellular transduction pathways, and pharmacological properties [2].

Indirect glutamate-induced neurotransmissions via postsynaptic group I (mGluR1 and

mGluR5) metabotropic glutamate receptors cause polyphosphoinositide hydrolysis by the formation of inositol 1,4,5-triphosphate and diacylglycerol as second messengers, with subsequent intracellular calcium release and protein kinase C activation [3-5]. Through these indirect excitatory neurotransmission pathways, mGluR1 and mGluR5 can trigger signaling cascades and modulate the activity of ion- and ligand-gated channels. Although mGluR1 and mGluR5 are highly homologous, they have distinct levels of expression, distribution, and function in the CNS [6-10]. Interestingly, inhibition of mGluR1 activation has been indicated as potentially useful for neuroprotection against

## PET study of $^{11}\text{C}$ -ITMM and $^{11}\text{C}$ -ITDM in monkey brain

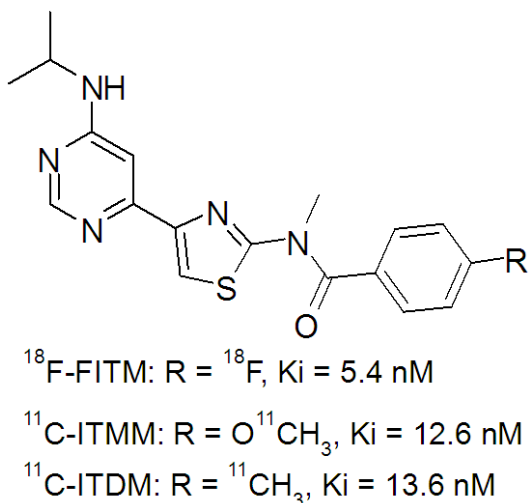


**Figure 1.** Chemical structures and *in vitro* binding affinities of  $^{18}\text{F}$ -FITM,  $^{11}\text{C}$ -ITMM, and  $^{11}\text{C}$ -ITDM for mGluR1.

various brain injuries, such as stroke [11-16], Parkinson disease [17-19], and Huntington disease [20]. As such, the ability to monitor mGluR1 as a biomarker would provide a greater understanding of its pathophysiological, psychophysiological, and biological roles.

We previously developed several promising  $^{11}\text{C}$  and  $^{18}\text{F}$ -labeled PET probes (**Figure 1**) for imaging of mGluR1 in the brain [21-23]. Of these, *N*-[4-[6-(isopropylamino)pyrimidin-4-yl]-1,3-thiazol-2-yl]-4- $^{11}\text{C}$ -methoxy-*N*-methylbenzamide ( $^{11}\text{C}$ -ITMM) was modified from 4- $^{18}\text{F}$ -fluoro-*N*-[4-[6-(isopropylamino)pyrimidin-4-yl]-1,3-thiazol-2-yl]-*N*-methylbenzamide ( $^{18}\text{F}$ -FITM), a highly selective radioligand for mGluR1 and successfully translated to human clinical studies [24, 25]. Although the *in vitro* binding affinity of ITMM ( $K_i$  = 12.6 nM) for mGluR1 was weaker than that of the parent compound FITM ( $K_i$  = 5.4 nM), PET analysis in the rat indicated that  $^{11}\text{C}$ -ITMM underwent relatively moderate clearance from mGluR1 in the brain with improved brain kinetics over  $^{18}\text{F}$ -FITM [22]. Based on these data,  $^{11}\text{C}$ -ITMM was progressed to a clinical study in humans [25]; however, the kinetics of  $^{11}\text{C}$ -ITMM in the human brain showed slow clearance following a peak at 15 min after injection. As such, PET quantitative analysis with  $^{11}\text{C}$ -ITMM for estimation of its specific binding to mGluR1 remains difficult.

We recently developed *N*-[4-[6-(isopropylamino)pyrimidin-4-yl]-1,3-thiazol-2-yl]-*N*-methyl-4- $^{11}\text{C}$ -methylbenzamide ( $^{11}\text{C}$ -ITDM) with an

$^{11}\text{C}$ -methyl group replacing the  $^{18}\text{F}$ -fluoro or  $^{11}\text{C}$ -methoxy group in  $^{18}\text{F}$ -FITM or  $^{11}\text{C}$ -ITMM (**Figure 1**) [21]. The *in vitro* binding affinity of  $^{11}\text{C}$ -ITDM ( $K_i$  = 13.6 nM) was similar to that of  $^{11}\text{C}$ -ITMM, while it showed faster clearance of radioactivity in the monkey when compared with  $^{11}\text{C}$ -ITMM in the human [21]. In addition, the uptake of  $^{11}\text{C}$ -ITDM in the pons, a region with negligible mGluR1 expression, was very low, at a similar level to tTAC in the monkey brain following specific mGluR1 blockade. These data strongly suggested that  $^{11}\text{C}$ -ITDM PET can acquire brain uptakes without perturbing the reference region. Therefore,  $^{11}\text{C}$ -ITDM would be an adequate PET ligand for quantitative analysis of mGluR1.

To aid in the progression of  $^{11}\text{C}$ -ITDM-PET toward clinical use in humans, we first performed a PET study on monkey with  $^{11}\text{C}$ -ITMM and  $^{11}\text{C}$ -ITDM to compare their brain kinetics.

### Materials and methods

#### Production of radioligands

$^{11}\text{C}$ -ITMM was synthesized by *O*- $^{11}\text{C}$ -methylation of a desmethyl precursor with  $^{11}\text{C}$ -iodomethane in the presence of sodium hydroxide at 70°C for 5 min in *N,N*-dimethylformamide [22]. At the end of synthesis,  $2.4 \pm 0.4$  GBq of  $^{11}\text{C}$ -ITMM was obtained with > 99% radiochemical purity and  $111.9 \pm 3.1$  GBq/ $\mu\text{mol}$  specific activity using  $19.9 \pm 1.2$  GBq of  $^{11}\text{C}$ -carbon dioxide ( $n = 3$ ).

$^{11}\text{C}$ -ITDM was synthesized by *C*- $^{11}\text{C}$ -methylation of an arylstannane precursor with  $^{11}\text{C}$ -iodomethane in the presence of tris(*o*-benzylideneacetone)dipalladium(0) and tri(*o*-tolyl)phosphine at 80°C for 5 min in *N,N*-dimethylformamide [21]. At the end of synthesis,  $1.4 \pm 0.1$  GBq of  $^{11}\text{C}$ -ITDM was obtained with > 99% radiochemical purity and  $70.3 \pm 3.0$  GBq/ $\mu\text{mol}$  specific activity using  $20.1 \pm 0.3$  GBq of  $^{11}\text{C}$ -carbon dioxide ( $n = 3$ ).

#### PET studies

A male rhesus monkey (5-6 kg) was purchased from the Central Institute for Experimental Animals (Kanagawa, Japan), and was maintained, handled, and used for experiments according to the recommendations of the Committee for the Care and Use of Laboratory Animals, National Institute of Radiological Sciences.

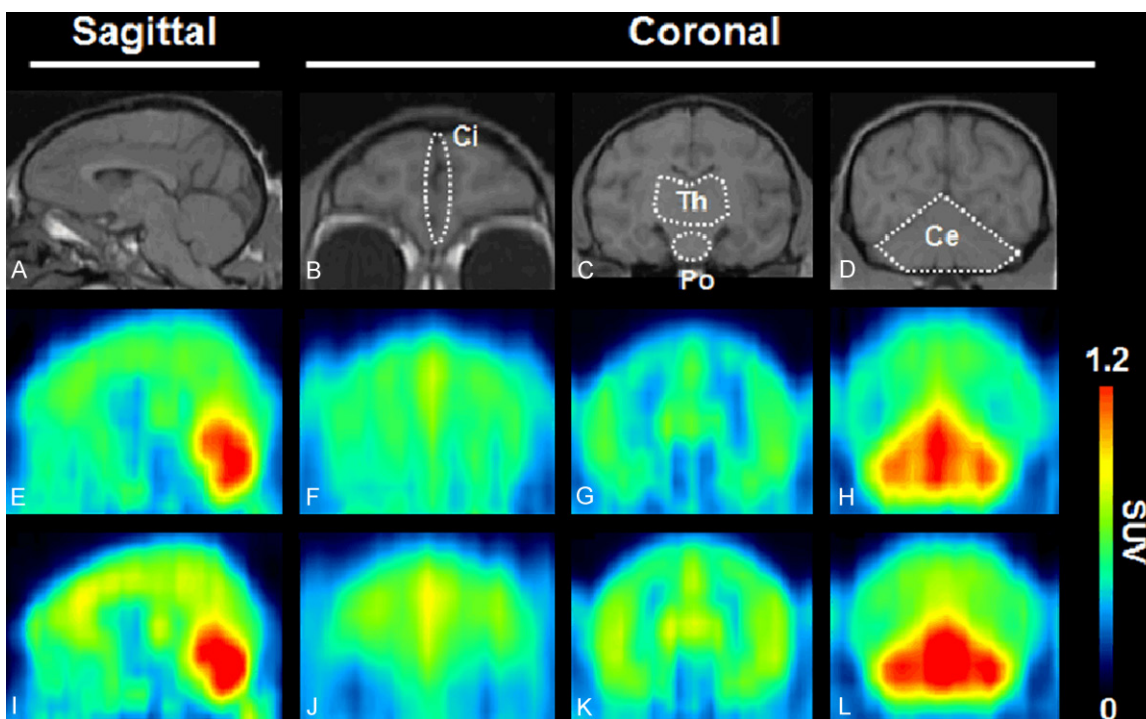


**Figure 2.** MRI and summed (10-90 min) PET images in the monkey brain. Prior to PET assessment, a monkey was scanned via high-resolution MRI (A-D). PET scans with  $^{11}\text{C}$ -ITMM (E-H) or  $^{11}\text{C}$ -ITDM (I-L) were performed on the same monkey. The tomograms were reconstructed in sagittal or coronal planes. Abbreviations: Ci, cingulate cortex; Th, thalamus; Po, pons; Ce, cerebellum.

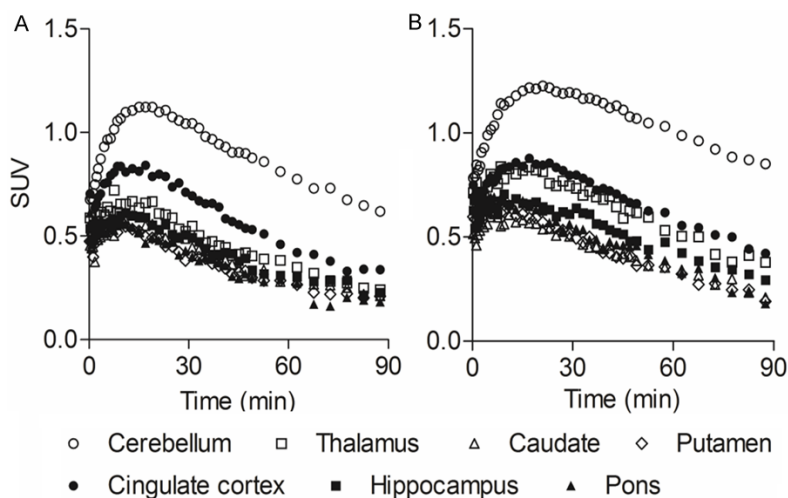


**Figure 3.** Time-activity curves of  $^{11}\text{C}$ -ITMM (A) and  $^{11}\text{C}$ -ITDM (B) in brain regions. Regions of interest were drawn on the cerebellum (open circles), thalamus (open squares), caudate (open triangles), putamen (open diamonds), cingulate cortex (solid circles), hippocampus (solid squares), and pons (solid triangles). The uptakes were expressed as SUV.

Prior to the PET assessments, magnetic resonance imaging (MRI) of the monkey's brain was performed with a 3.0 T scanner (Signa Excite HD, GE Medical Systems, Milwaukee WI, USA)

using a short time inversion recovery sequence (repetition time = 5000 ms, echo time = 80 ms, inversion time = 110 ms, field of view = 100 mm, number of slices = 52, slice thickness = 1 mm without slice gap, 512 × 384 acquisition matrix, which after reconstruction was reformatted to a 512 × 512 image matrix, number of excitations = 6, total acquisition time = 72 min).

PET scans were performed using a high-resolution SHR-7700 PET camera (Hamamatsu Photonics, Shizuoka, Japan) designed for laboratory animals. A solution containing  $^{11}\text{C}$ -ITMM (172 MBq, 1.8 nmol, 0.3 mL) or  $^{11}\text{C}$ -ITDM (185 MBq, 5.0 nmol, 0.5 mL) was injected intravenously into the monkey, which was immobilized in a homemade chamber, and dynamic tomographic

## PET study of $^{11}\text{C}$ -ITMM and $^{11}\text{C}$ -ITDM in monkey brain

**Table 1.** Percentage of radioactivity in monkey plasma at 1, 5, 15, 30, 60, and 90 min after injection of  $^{11}\text{C}$ -ITMM or  $^{11}\text{C}$ -ITDM

Time after the injection (min)	$^{11}\text{C}$ -ITMM			$^{11}\text{C}$ -ITDM		
	% of total radioactivity					
	Metabolite 1	Metabolite 2	Parent	Metabolite 1	Metabolite 2	Parent
1	0.1	0.0	99.9	0.8	0.1	99.2
5	8.9	2.5	88.6	18.9	3.2	78.0
15	33.0	8.2	58.8	35.4	6.7	57.9
30	46.3	14.6	39.1	40.0	6.9	53.2
60	50.6	17.6	31.8	52.7	9.0	38.3
90	52.0	17.5	30.4	49.3	12.3	38.4

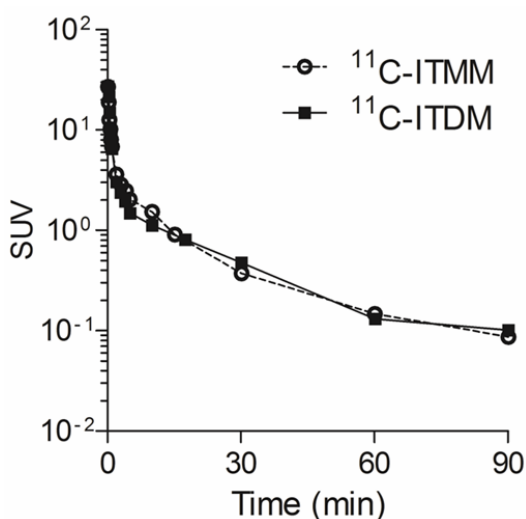


**Figure 4.** Input curves of  $^{11}\text{C}$ -ITMM (open circles) and  $^{11}\text{C}$ -ITDM (solid squares) in monkey plasma. The radioactivities were expressed as SUV.

scanning was performed for 90 min (30 s  $\times$  7 frames, 60 s  $\times$  7 frames, 120 s  $\times$  20 frames, and 300 s  $\times$  8 frames).

### Metabolite analysis of blood samples

Arterial blood (0.5-1 mL) was manually sampled at 10, 20, 30, 40, 50 s, 1, 2, 3, 4, 5, 10, 15, 30, 60, and 90 min after injection. The radioactivity in the whole blood and plasma was counted using a 1480 Wizard autogamma scintillation counter (Perkin-Elmer, Waltham, MA, USA). Radioactivity was corrected for decay. Whole blood (0.5-1.5 mL) samples were centrifuged at 20,000 g for 1 min at 4°C to separate the plasma. The supernatant (0.5 mL) was then collected in a test tube containing acetonitrile (0.5 mL), and the resulting mixture was vortexed for 15 s and centrifuged at 20,000 g for 2 min at 4°C for deproteinization. An aliquot of the

supernatant obtained from the plasma was injected into a high-performance liquid chromatography (HPLC) system with a radiation detector [26], and then analyzed using a Capcell Pack  $\text{C}_{18}$  column (4.6 mm i.d.  $\times$  250 mm; Shiseido, Tokyo, Japan) with a mixture of acetonitrile, water, and triethylamine (6/4/0.01 for  $^{11}\text{C}$ -ITMM; 7/3/0.01 for  $^{11}\text{C}$ -ITDM). The percentage of  $^{11}\text{C}$ -ITMM (retention time = 5.3 min at 1.5 mL $\cdot$ min $^{-1}$ ) or  $^{11}\text{C}$ -ITDM (retention time = 7.1 min at 1.0 mL $\cdot$ min $^{-1}$ ) to total radioactivity (corrected for decay) on the HPLC charts was calculated as percentage of intact = (peak area of intact/total peak area)  $\times$  100.

### Kinetic analysis

All PET images were generated by averaging the uptakes between 10 and 90 min. Volumes of interest (VOIs) were placed on each brain region using PMOD version 3.2 image analysis software (PMOD Technologies, Zurich, Switzerland) with reference to the MRI template. Each PET image was manually overlain on the MRI template, and the tissue time-activity curves (tTACs) in each VOI were generated. Brain uptake was decay corrected to the injection time and expressed as the standardized uptake value (SUV), which was normalized to the injected radioactivity and body weight [27].

The plasma input function was obtained from the plasma fraction corrected by metabolite analysis using the PMOD (PMOD Technologies). All kinetic parameters in the cerebellum, thalamus, caudate, putamen, cingulate cortex, hippocampus, and pons were generated by nonlinear-least-square fitting with the two-tissue compartment model (2-TCM). The six parameters were: plasma-to-tissue influx and efflux rate constants,  $K_1$  and  $k_2$ ; the ligand binding

## PET study of $^{11}\text{C}$ -ITMM and $^{11}\text{C}$ -ITDM in monkey brain

**Table 2.** Kinetic parameters obtained by 2-TCM in PET with  $^{11}\text{C}$ -ITMM

Parameter	Cerebellum		Thalamus		Caudate		Putamen		Cingulate cortex		Hippocampus		Pons	
	Mean	%COV	Mean	%COV	Mean	%COV	Mean	%COV	Mean	%COV	Mean	%COV	Mean	%COV
$K_1$ (mLcm $^{-3}$ min $^{-1}$ )	0.052	3.0	0.061	7.9	0.043	6.3	0.042	4.2	0.106	13.2	0.092	11.7	0.168	18.2
$k_2$ (min $^{-1}$ )	0.105	13.4	0.433	19.9	0.317	16.7	0.251	11.4	1.275	25.0	1.243	20.3	2.943	24.9
$k_3$ (min $^{-1}$ )	0.099	15.1	0.201	15.2	0.147	14.9	0.111	12.2	0.441	12.6	0.332	10.9	0.378	12.2
$k_4$ (min $^{-1}$ )	0.025	7.8	0.031	7.2	0.028	8.0	0.030	7.1	0.031	6.2	0.029	5.9	0.032	7.0
$V_T$ (mLcm $^{-3}$ )	2.5	3.2	1.0	3.0	0.9	3.4	0.8	2.7	1.3	2.3	0.9	2.7	0.7	3.5
AUC (SUV·min)	88.4	—	49.3	—	39.2	—	37.3	—	60.5	—	45.0	—	38.4	—

**Table 3.** Kinetic parameters obtained by 2-TCM in PET with  $^{11}\text{C}$ -ITDM

Parameter	Cerebellum		Thalamus		Caudate		Putamen		Cingulate cortex		Hippocampus		Pons	
	Mean	%COV	Mean	%COV	Mean	%COV	Mean	%COV	Mean	%COV	Mean	%COV	Mean	%COV
$K_1$ (mLcm $^{-3}$ min $^{-1}$ )	0.045	1.6	0.049	6.7	0.027	2.6	0.032	1.9	0.059	9.8	0.032	2.7	0.036	3.7
$k_2$ (min $^{-1}$ )	0.030	12.2	0.312	29.7	0.054	13.1	0.075	8.3	0.825	32.8	0.071	15.6	0.095	17.2
$k_3$ (min $^{-1}$ )	0.026	37.0	0.377	22.9	0.028	42.8	0.037	22.2	0.832	17.8	0.066	30.2	0.065	33.6
$k_4$ (min $^{-1}$ )	0.019	37.8	0.052	8.6	0.031	31.6	0.036	14.8	0.043	9.9	0.044	14.4	0.045	17.4
$V_T$ (mLcm $^{-3}$ )	3.6	10.9	1.3	1.7	0.9	5.4	0.9	2.7	1.5	1.3	1.1	2.7	0.9	3.3
AUC (SUV·min)	94.2	—	55.0	—	37.4	—	37.7	—	59.4	—	45.5	—	40.6	—

rate on and off the receptors,  $k_3$  and  $k_4$ ; the volume of distribution,  $V_T = (K_1/k_2) (1 + k_3/k_4)$ ; and the area under the curve (AUC). The distribution volume ratio (DVR) in each region was acquired using  $V_T$  of the pons as a reference region, where mGluR1 expression is negligible [8]. The DVR of the target region was calculated as:  $\text{DVR} = V_T(\text{region})/V_T(\text{pons})$ . The ability to identify the parameters was expressed by coefficients of variation (%COV). Blood volume in the monkey brain was fixed at 3% according to a previous report [28].

To validate the efficacy of the reference tissue model, the binding potential ( $\text{BP}_{\text{ND}}$ ) values based on general reference tissue methods were compared with DVR-1 values based on the 2-TCM. The  $\text{BP}_{\text{ND}}$  values based on the simplified reference tissue model (SRTM) [29], Ichise's multilinear reference tissue model (MRTM) [30], or Logan's reference tissue model (Logan R) [31] were acquired using tTAC of the pons as a reference region. The analysis based on Logan R were performed using average  $k_2'$ , which has been obtained from the  $k_2$  value of the pons based on 1-TCM.

### Results

#### PET studies

**Figure 2** shows PET images with  $^{11}\text{C}$ -ITMM (E-H) and  $^{11}\text{C}$ -ITDM (I-L) in the monkey brain. Uptake

of  $^{11}\text{C}$ -ITDM in the brain seemed slightly higher than that of  $^{11}\text{C}$ -ITMM. In both PET images, the highest radioactive signal was found in the cerebellum, moderate uptake was detected in the thalamus and cingulate cortex, and low uptake was observed in the striatum and brainstem.

**Figure 3** shows the tTACs of  $^{11}\text{C}$ -ITMM (A) and  $^{11}\text{C}$ -ITDM (B) in various brain regions. The respective tTACs of the radioprobes peaked at 10-20 min for  $^{11}\text{C}$ -ITMM and 15-20 min for  $^{11}\text{C}$ -ITDM after a bolus injection, showing gradual clearance after that. The maximum of SUV in PET studies with  $^{11}\text{C}$ -ITMM or  $^{11}\text{C}$ -ITDM was 1.1 or 1.2 for the cerebellum, 0.7 or 0.8 for the thalamus, 0.6 or 0.6 for the caudate, 0.6 or 0.7 for the putamen, 0.8 or 0.9 for the cingulate cortex, 0.6 or 0.7 for the hippocampus, and 0.6 or 0.7 for the pons, respectively.

#### Input function in PET studies

**Table 1** shows the results of metabolite analyses in the monkey plasma.  $^{11}\text{C}$ -ITMM and  $^{11}\text{C}$ -ITDM were both gradually decomposed to radiolabeled metabolites following a bolus injection. At 90 min following injection, the percentage of parent compound was approximately 30% for  $^{11}\text{C}$ -ITMM and 40% for  $^{11}\text{C}$ -ITDM. Two unknown radiolabeled metabolites were detected at much a higher polarity than their corresponding intact forms.

## PET study of $^{11}\text{C}$ -ITMM and $^{11}\text{C}$ -ITDM in monkey brain

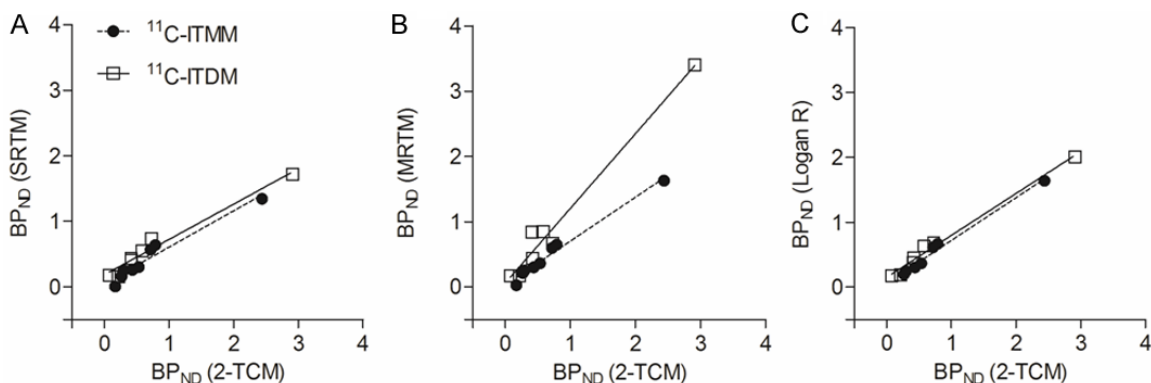


**Figure 5.** Correlation between  $\text{BP}_{\text{ND}}$  based on reference tissue model and DVR-1 based on 2-TCM in PET studies with  $^{11}\text{C}$ -ITMM (solid circles) or  $^{11}\text{C}$ -ITDM (open squares). Reference tissue models were used SRTM (A), MRTM (B), and Logan R (C).

**Table 4.** The slope of regression line and coefficient of determination ( $r^2$ ) in the correlational scatter plot of  $\text{BP}_{\text{ND}}$  based on reference tissue models against DVR-1 based on 2-TCM

Probe	SRTM			MRTM			Logan R		
	Slope	1/Slope	$r^2$	Slope	1/Slope	$r^2$	Slope	1/Slope	$r^2$
$^{11}\text{C}$ -ITMM	0.56	1.8	0.95	0.67	1.49	0.98	0.66	1.52	0.99
$^{11}\text{C}$ -ITDM	0.54	1.85	0.97	1.15	0.87	0.98	0.65	1.55	0.99

**Figure 4** shows metabolite-corrected input curves of plasma with  $^{11}\text{C}$ -ITMM or  $^{11}\text{C}$ -ITDM. Both input curves showed a rapid decrease following a bolus injection. At 30 min following injection, plasma activities for both probes were one-fiftieth of their peak.

### Kinetic analysis

**Tables 2** and **3** show the full kinetic parameters acquired by 2-TCM with  $^{11}\text{C}$ -ITMM and  $^{11}\text{C}$ -ITDM. The  $V_T$  values corresponding to bindings of radioligand and the AUC values indicating uptake of radioactivity in  $^{11}\text{C}$ -ITDM PET were superior to those in  $^{11}\text{C}$ -ITMM PET. All of the generated fitting curves showed high confidence ( $r^2 > 0.90$ ).

### Correlation between general reference tissue models and 2-TCM in PET with $^{11}\text{C}$ -ITMM or $^{11}\text{C}$ -ITDM

**Figure 5** shows correlational scatter plots between general reference tissue model-based  $\text{BP}_{\text{ND}}$ s and 2-TCM-based DVR-1 values in the quantitative PET analysis with  $^{11}\text{C}$ -ITMM or  $^{11}\text{C}$ -ITDM. **Table 4** shows the slope of a regression line and coefficient of determination in each brain region. The slope of regression lines

directly indicates under- or overestimation of  $\text{BP}_{\text{ND}}$  based on the reference tissue model when compared with DVR-1 based on the 2-TCM. As shown in **Figure 5** and **Table 4**,  $\text{BP}_{\text{ND}}$ s derived from

SRTM in both radiopharmaceuticals showed marked underestimation (slope was 0.56 for  $^{11}\text{C}$ -ITMM and 0.54 for  $^{11}\text{C}$ -ITDM) when compared with DVR-1 values calculated by 2-TCM (**Figure 5A**). In the MRTM-based  $\text{BP}_{\text{ND}}$ s, that of  $^{11}\text{C}$ -ITDM showed slight overestimation (slope was 1.15) against 2-TCM-based DVR-1 values, whereas that of  $^{11}\text{C}$ -ITMM was underestimated (slope was 0.67) (**Figure 5B**).  $\text{BP}_{\text{ND}}$ s based on Logan Ref in both radiopharmaceuticals showed relatively low underestimation (slope was 0.66 for  $^{11}\text{C}$ -ITMM and 0.65 for  $^{11}\text{C}$ -ITDM) against DVR-1 values calculated by 2-TCM (**Figure 5C**). The majority of regression lines of scatter plots exhibited with high correlation ( $r^2 > 0.95$ ).

**Figure 6** shows Bland-Altman plots between reference tissue models and 2-TCM in PET studies using  $^{11}\text{C}$ -ITMM or  $^{11}\text{C}$ -ITDM. There were no significant differences between general reference tissue models and 2-TCM in PET kinetic analysis using both radiopharmaceuticals. Bias of reference tissue model for  $^{11}\text{C}$ -ITMM or  $^{11}\text{C}$ -ITDM were  $39.2 \pm 15.5\%$  or  $1.49 \pm 40.3\%$ ,  $27.0 \pm 10.3\%$  or  $-23.9 \pm 37.0\%$ , and  $27.6 \pm 10.1\%$  or  $-3.8 \pm 34.7\%$  for the SRTM vs. 2-TCM, MRTM vs. 2-TCM, and Logan R vs. 2-TCM, respectively.

## PET study of $^{11}\text{C}$ -ITMM and $^{11}\text{C}$ -ITDM in monkey brain

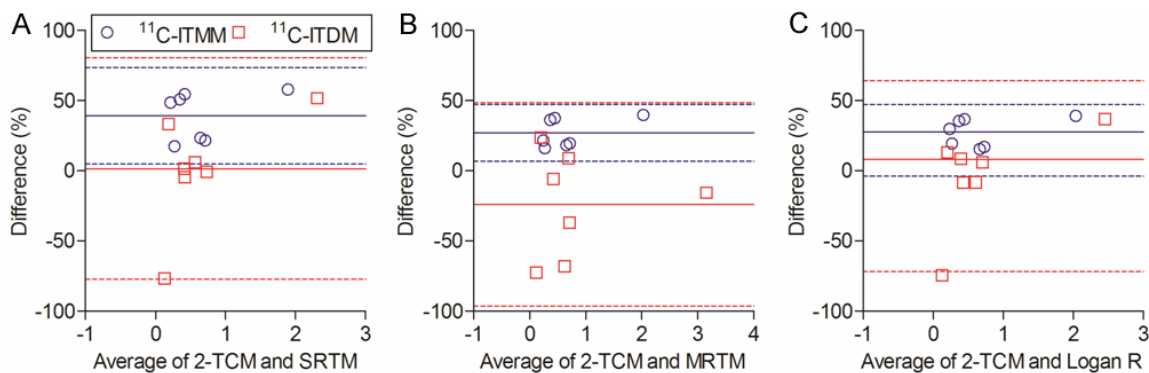


**Figure 6.** Bland-Altman plot between  $\text{BP}_{\text{ND}}$  based on reference tissue methods, which are SRTM (A), MRTM (B), and Logan R (C), and DVR-1 based on 2-TCM in PET studies with  $^{11}\text{C}$ -ITMM (blue circles) or  $^{11}\text{C}$ -ITDM (red squares).

### Discussion

In this study, we compared the results of quantitative PET analysis in the monkey brain between  $^{11}\text{C}$ -ITMM and  $^{11}\text{C}$ -ITDM. In respective PET images (**Figure 2**), heterogeneous uptake of radioactivity was found in brain regions corresponding to mGluR1 distribution with  $^{18}\text{F}$ -FITM in the monkey [32], suggesting that the uptake of radioactivity in the PET images for both radiopharmaceuticals reflected their binding to mGluR1. The uptake of  $^{11}\text{C}$ -ITDM was slightly higher than that of  $^{11}\text{C}$ -ITMM, although the brain kinetics of both radiopharmaceuticals showed a similar rapid clearance following a peak uptake at approximately 15 min after injection (**Figure 3**). Surprisingly, although the tTACs of  $^{11}\text{C}$ -ITMM in a human showed a slow clearance after peaking at 15 min [25], the tTACs of  $^{11}\text{C}$ -ITMM in the monkey were more rapid. These differences in brain kinetics of  $^{11}\text{C}$ -ITMM between the monkey and human may be caused by a difference in enzymatic metabolism of  $^{11}\text{C}$ -ITMM *in vivo*. This difference is also seen in the kinetic analysis of other PET radiopharmaceuticals. For example, the metabolization rate of  $^{11}\text{C}$ -Ro15-4513, a selective probe for a central benzodiazepine receptor, was reported to be caused by enzymatic hydrolysis of  $^{11}\text{C}$ -Ro15-4513 to differing degrees in the blood of several species: mouse < rat < human < monkey [33]. In the case of  $^{11}\text{C}$ -ITMM, the percentage of unchanged form in the plasma at 60 min after injection was 62% in the human [25] and 31% in the monkey. Thus, differences in enzyme activity *in vivo* may contribute to differences in metabolization rate of  $^{11}\text{C}$ -ITMM in the human and monkey, resulting in different input functions in brain tissues. Indeed, the

maximum uptake of  $^{11}\text{C}$ -ITMM in the cerebellum was 2.5 SUV for human and 1.1 SUV for monkey. In addition to differences in enzyme activity, there are also differences in mGluR1 density among different species. In a binding study with  $^{18}\text{F}$ -MK-1312, a radioligand for mGluR1, the density ( $B_{\text{max}}$ ) of mGluR1 in the cerebellum was reported to be 82 nM for human and 53 nM for monkey [34]. Considering these findings, differences in mGluR1 density in the peripheral organs are not surprising. Because of these differences, the brain uptake and clearance of  $^{11}\text{C}$ -ITMM in human may be higher and slower, respectively, when compared with the monkey.

Although mGluR1 density is different between human and monkey brains, the distribution pattern is very similar in both species. We previously assessed the distribution pattern of mGluR1 in rodents (mouse and rat) and primates (monkey and human) [21-23, 35], and found that mGluR1 density in rodent brains was relatively high in the thalamus, striatum, and hippocampus, while high expression of mGluR1 in primate brains was highest in the cerebral cortex followed by the cerebellum, the region with the highest density of this receptor in both rodent and primate brains. Considering these profiles, quantitative PET analysis for mGluR1 in the monkey brain would be a suitable simulation for progression toward clinical studies in humans.

The variation of the  $V_{\text{T}}$  values based on 2-TCM in brain regions was between 0.7-2.5  $\text{mL}\cdot\text{cm}^{-3}$  for  $^{11}\text{C}$ -ITMM and 0.9-3.6  $\text{mL}\cdot\text{cm}^{-3}$  for  $^{11}\text{C}$ -ITDM (**Tables 2** and **3**). However, the variation of  $V_{\text{T}}$  values for  $^{18}\text{F}$ -FITM was reported to be 2.4-11.5

$\text{mL}\cdot\text{cm}^{-3}$  in monkey brain regions [32]. Importantly, although the corresponding  $V_T$  value for both radioligands was lower than that of  $^{18}\text{F}$ -FITM, their  $V_T$  values in the pons, a mGluR1-negligible region, were similar to the reference rather than the plasma input function for  $^{18}\text{F}$ -FITM; i.e., the  $V_T$  in the pons was  $0.7 \text{ mL}\cdot\text{cm}^{-3}$  for  $^{11}\text{C}$ -ITMM,  $0.9 \text{ mL}\cdot\text{cm}^{-3}$  for  $^{11}\text{C}$ -ITDM, and  $2.4 \text{ mL}\cdot\text{cm}^{-3}$  for  $^{18}\text{F}$ -FITM. These data strongly suggest that tTACs in the pons of  $^{11}\text{C}$ -ITMM and  $^{11}\text{C}$ -ITDM would be suitable as the reference. In fact, the pons is often used as a reference region instead of the plasma input function in quantitative PET analysis of neuroreceptors [36, 37].

To validate the usefulness of the reference tissue model using tTAC of the pons, we confirmed the relationship between  $\text{BP}_{\text{ND}}$ s based on several reference tissue models and DVR-1 based on 2-TCM in PET studies with  $^{11}\text{C}$ -ITMM or  $^{11}\text{C}$ -ITDM. Among the scattergrams (Figure 5), all of the slopes of regression lines for  $^{11}\text{C}$ -ITMM showed underestimations of reference tissue models against 2-TCM, whereas the slope of the regression line of  $^{11}\text{C}$ -ITDM with MRTM showed slight overestimation, despite the slopes of the regression lines of  $^{11}\text{C}$ -ITDM with SRTM or Logan R indicating underestimation similar to that with  $^{11}\text{C}$ -ITMM. Although  $\text{BP}_{\text{ND}}$ s based on reference tissue models using alternative PET probes were under- or overestimated compared with 2-TCM, there were no significant differences between the two kinetic models. Thus, noninvasive PET quantitative analysis using a reference tissue for both radioprobes is feasible, and the blood sampling method is not required.

### Conclusion

We performed quantitative PET analysis of  $^{11}\text{C}$ -ITDM binding to mGluR1 in the monkey. We validated that PET with  $^{11}\text{C}$ -ITMM or  $^{11}\text{C}$ -ITDM can use reference tissue models instead of the blood sampling method. Therefore, noninvasive kinetic analysis using reference tissue models in  $^{11}\text{C}$ -ITDM PET is a candidate for clinical studies using human subjects.

### Acknowledgements

We thank the staff at the National Institute of Radiological Sciences for their support with the cyclotron operation, radioisotope production, radiosynthesis, and animal experiments.

### Disclosure of conflict of interest

The authors declare no conflict of interest.

**Address correspondence to:** Dr. Ming-Rong Zhang, Molecular Probe Program, Molecular Imaging Center, National Institute of Radiological Sciences, 4-9-1 Anagawa, Inage-ku, Chiba 263-8555, Japan. Tel: +81 43 382 3709; Fax: +81 43 206 3261; E-mail: zhang@nirs.go.jp (MRZ); yamato@nirs.go.jp (TY)

### References

- [1] Hermans E and Challiss RA. Structural, signaling and regulatory properties of the group I metabotropic glutamate receptors: prototypic family C G-protein-coupled receptors. *Biochem J* 2001; 359: 465-484.
- [2] Ferraguti F, Crepaldi L, Nicoletti F. Metabotropic glutamate 1 receptor: current concepts and perspectives. *Pharmacol Rev* 2008; 60: 536-581.
- [3] Aramori I and Nakanishi S. Signal transduction and pharmacological characteristics of a metabotropic glutamate receptor, mGluR1, in transfected CHO cells. *Neuron* 1992; 8: 757-765.
- [4] Di Matteo V, De Blasi A, Di Giulio C, Esposito E. Role of 5-HT(2C) receptors in the control of central dopamine function. *Trends Pharmacol Sci* 2001; 22: 229-232.
- [5] Francesconi A and Duvoisin RM. Role of the second and third intracellular loops of metabotropic glutamate receptors in mediating dual signal transduction activation. *J Biol Chem* 1998; 273: 5615-5624.
- [6] Battaglia G, Bruno V, Pisani A, Centonze D, Catania MV, Calabresi P, Nicoletti F. Selective blockade of type-1 metabotropic glutamate receptors induces neuroprotection by enhancing gabaergic transmission. *Mol Cell Neurosci* 2001; 17: 1071-1083.
- [7] Bordi F and Ugolini A. Group I metabotropic glutamate receptors: implications for brain diseases. *Prog Neurobiol* 1999; 59: 55-79.
- [8] Fotuhi M, Sharp AH, Glatt CE, Hwang PM, von Krosigk M, Snyder SH, Dawson TM. Differential localization of phosphoinositide-linked metabotropic glutamate receptor (mGluR1) and the inositol 1,4,5-trisphosphate receptor in rat brain. *J Neurosci* 1993; 13: 2001-2012.
- [9] Pisani A, Calabresi P, Centonze D, Bernardi G. Enhancement of NMDA responses by group I metabotropic glutamate receptor activation in striatal neurones. *Br J Pharmacol* 1997; 120: 1007-1014.
- [10] Valenti O, Conn PJ, Marino MJ. Distinct physiological roles of the Gq-coupled metabotropic

## PET study of $^{11}\text{C}$ -ITMM and $^{11}\text{C}$ -ITDM in monkey brain

- glutamate receptors Co-expressed in the same neuronal populations. *J Cell Physiol* 2002; 191: 125-137.
- [11] De Vry J, Horvath E, Schreiber R. Neuroprotective and behavioral effects of the selective metabotropic glutamate mGlu(1) receptor antagonist BAY 36-7620. *Eur J Pharmacol* 2001; 428: 203-214.
- [12] Kohara A, Takahashi M, Yatsugi S, Tamura S, Shitaka Y, Hayashibe S, Kawabata S, Okada M. Neuroprotective effects of the selective type 1 metabotropic glutamate receptor antagonist YM-202074 in rat stroke models. *Brain Res* 2008; 1191: 168-179.
- [13] Moroni F, Attucci S, Cozzi A, Meli E, Picca R, Scheideler MA, Pellicciari R, Noe C, Sarichelou L, Pellegrini-Giampietro DE. The novel and systemically active metabotropic glutamate 1 (mGlu1) receptor antagonist 3-MATIDA reduces post-ischemic neuronal death. *Neuropharmacology* 2002; 42: 741-751.
- [14] Murotomi K, Takagi N, Takayanagi G, Ono M, Takeo S, Tananaka K. mGluR1 antagonist decreases tyrosine phosphorylation of NMDA receptor and attenuates infarct size after transient focal cerebral ischemia. *J Neurochem* 2008; 105: 1625-1634.
- [15] Szydłowska K, Kaminska B, Baude A, Parsons CG, Danysz W. Neuroprotective activity of selective mGlu1 and mGlu5 antagonists in vitro and in vivo. *Eur J Pharmacol* 2007; 554: 18-29.
- [16] Zhou M, Xu W, Liao G, Bi X, Baudry M. Neuroprotection against neonatal hypoxia/ischemia-induced cerebral cell death by prevention of calpain-mediated mGluR1 $\alpha$  truncation. *Exp Neurol* 2009; 218: 75-82.
- [17] Dekundy A, Pietraszek M, Schaefer D, Cenci MA, Danysz W. Effects of group I metabotropic glutamate receptors blockade in experimental models of Parkinson's disease. *Brain Res Bull* 2006; 69: 318-326.
- [18] Kaneda K, Tachibana Y, Imanishi M, Kita H, Shigemoto R, Nambu A, Takada M. Down-regulation of metabotropic glutamate receptor 1  $\alpha$  in globus pallidus and substantia nigra of Parkinsonian monkeys. *Eur J Neurosci* 2005; 22: 3241-3254.
- [19] Ossowska K, Wardas J, Pietraszek M, Konieczny J, Wolfarth S. The striopallidal pathway is involved in antiparkinsonian-like effects of the blockade of group I metabotropic glutamate receptors in rats. *Neurosci Lett* 2003; 342: 21-24.
- [20] Ribeiro FM, Paquet M, Ferreira LT, Cregan T, Swan P, Cregan SP, Ferguson SS. Metabotropic glutamate receptor-mediated cell signaling pathways are altered in a mouse model of Huntington's disease. *J Neurosci* 2010; 30: 316-324.
- [21] Fujinaga M, Yamasaki T, Maeda J, Yui J, Xie L, Nagai Y, Nengaki N, Hatori A, Kumata K, Kawamura K, Zhang MR. Development of N-[4-[6-(isopropylamino)pyrimidin-4-yl]-1,3-thiazol-2-yl]-N-methyl-4- $^{11}\text{C}$ -methylbenzamide for positron emission tomography imaging of metabotropic glutamate 1 receptor in monkey brain. *J Med Chem* 2012; 55: 11042-11051.
- [22] Fujinaga M, Yamasaki T, Yui J, Hatori A, Xie L, Kawamura K, Asakawa C, Kumata K, Yoshida Y, Ogawa M, Nengaki N, Fukumura T, Zhang MR. Synthesis and evaluation of novel radioligands for positron emission tomography imaging of metabotropic glutamate receptor subtype 1 (mGluR1) in rodent brain. *J Med Chem* 2012; 55: 2342-2352.
- [23] Yamasaki T, Fujinaga M, Yoshida Y, Kumata K, Yui J, Kawamura K, Hatori A, Fukumura T, Zhang MR. Radiosynthesis and preliminary evaluation of 4- $^{18}\text{F}$ -fluoro-N-[4-[6-(isopropylamino)pyrimidin-4-yl]-1,3-thiazol-2-yl]-N-methylbenzamide as a new positron emission tomography ligand for metabotropic glutamate receptor subtype 1. *Bioorg Med Chem Lett* 2011; 21: 2998-3001.
- [24] Toyohara J, Sakata M, Fujinaga M, Yamasaki T, Oda K, Ishii K, Zhang MR, Moriguchi Jeckel CM, Ishiwata K. Preclinical and the first clinical studies on  $^{11}\text{C}$ -ITMM for mapping metabotropic glutamate receptor subtype 1 by positron emission tomography. *Nucl Med Biol* 2013; 40: 214-220.
- [25] Toyohara J, Sakata M, Oda K, Ishii K, Ito K, Hiura M, Fujinaga M, Yamasaki T, Zhang MR, Ishiwata K. Initial human PET studies of metabotropic glutamate receptor type 1 ligand  $^{11}\text{C}$ -ITMM. *J Nucl Med* 2013; 54: 1-6.
- [26] Takei M, Kida T, Suzuki K. Sensitive measurement of positron emitters eluted from HPLC. *Appl Radiat Isot* 2001; 55: 229-234.
- [27] Keyes JW Jr. SUV: standard uptake or silly useless value? *J Nucl Med* 1995; 36: 1836-1839.
- [28] Ohya T, Okamura T, Nagai Y, Fukushi K, Irie T, Suhara T, Zhang MR, Fukumura T, Kikuchi T. Effect of radiolabeled metabolite elimination from the brain on the accuracy of cerebral enzyme activity estimation using positron emission tomography with substrate tracers. *Neuroimage* 2011; 56: 105-1110.
- [29] Lammertsma AA and Hume SP. Simplified reference tissue model for PET receptor studies. *Neuroimage* 1996; 4: 153-158.
- [30] Ichise M, Liow JS, Lu JQ, Takano A, Model K, Toyama H, Suhara T, Suzuki K, Innis RB, Carson RE. Linearized reference tissue parametric imaging methods: application to  $^{11}\text{C}$ -DASB positron emission tomography studies of the serotonin transporter in human brain. *J Cereb Blood Flow Metab* 2003; 23: 1096-1112.

## PET study of $^{11}\text{C}$ -ITMM and $^{11}\text{C}$ -ITDM in monkey brain

- [31] Logan J, Fowler JS, Volkow ND, Wang GJ, Ding YS, Alexoff DL. Distribution volume ratios without blood sampling from graphical analysis of PET data. *J Cereb Blood Flow Metab* 1996; 16: 834-840.
- [32] Yamasaki T, Fujinaga M, Maeda J, Kawamura K, Yui J, Hatori A, Yoshida Y, Nagai Y, Tokunaga M, Higuchi M, Suhara T, Fukumura T, Zhang MR. Imaging for metabotropic glutamate receptor subtype 1 in rat and monkey brains using PET with  $^{18}\text{F}$ -FITM. *Eur J Nucl Med Mol Imaging* 2012; 39: 632-641.
- [33] Kida T, Noguchi J, Zhang MR, Suhara T, Suzuki K. Metabolite analysis of  $^{11}\text{C}$ -Ro15-4513 in mice, rats, monkeys and humans. *Nucl Med Biol* 2003; 30: 779-784.
- [34] Hostetler ED, Eng W, Joshi AD, Sanabria-Borhquez S, Kawamoto H, Ito S, O'Malley S, Krause S, Ryan C, Patel S, Williams M, Riffel K, Suzuki G, Ozaki S, Ohta H, Cook J, Burns HD, Hargreaves R. Synthesis, characterization, and monkey PET studies of  $^{18}\text{F}$ -MK-1312, a PET tracer for quantification of mGluR1 receptor occupancy by MK-5435. *Synapse* 2011; 65: 125-135.
- [35] Fujinaga M, Maeda J, Yui J, Hatori A, Yamasaki T, Kawamura K, Kumata K, Yoshida Y, Nagai Y, Higuchi M, Suhara T, Fukumura T, Zhang MR. Characterization of 1-(2- $^{18}\text{F}$ -fluoro-3-pyridyl)-4-(2-isopropyl-1-oxo-isoindoline-5-yl)-5-methyl-1H-1,2,3-triazole, a PET ligand for imaging the metabotropic glutamate receptor type 1 in rat and monkey brains. *J Neurochem* 2012; 121: 115-124.
- [36] Geeraerts T, Coles JP, Aigbirhio FI, Pickard JD, Menon DK, Fryer TD, Hong YT. Validation of reference tissue modelling for  $^{11}\text{C}$ -flumazenil positron emission tomography following head injury. *Ann Nucl Med* 2011; 25: 396-405.
- [37] Pearl PL, Gibson KM, Quezaso Z, Dustin I, Taylor J, Trzcinski S, Schreiber J, Forester K, Reeves-Tyer P, Liew C, Shamim S, Herscovitch P, Carson R, Butman J, Jacobs C, Theodore W. Decreased GABA-A binding on FMZ-PET in succinic semialdehyde dehydrogenase deficiency. *Neurology* 2009; 73: 423-429.